Journal of The Electrochemical Society, **152** (1) A1-A5 (2005)
0013-4651/2004/152(1)/A1/5/$7.00 © The Electrochemical Society, Inc.

Rubbery Graft Copolymer Electrolytes for Solid-State, Thin-Film Lithium Batteries

Patrick E. Trapa,[a,*] You-Yeon Won,[a] Simon C. Mui,[a,*] Elsa A. Olivetti,[a] Biying Huang,[a] Donald R. Sadoway,[a,*] Anne M. Mayes,[a,*,z] and Steven Dallek[b]

[a]*Department of Materials Science and Engineering, Massachusetts Institute of Technology, Cambridge, Massachusetts, 02139-4307, USA*
[b]*Naval Surface Warfare Center, Carderock Division, West Bethesda, Maryland, 20817, USA*

Graft copolymer electrolytes (GCEs) of poly[(oxyethylene)$_9$ methacrylate]-*g*-poly(dimethyl siloxane) (POEM-*g*-PDMS) (70:30) have been synthesized by simple free radical polymerization using a macromonomer route. Differential scanning calorimetry, transmission electron microscopy, and small angle neutron scattering confirmed the material to be microphase-separated with a domain periodicity of ~25 nm. Over the temperature range $290 < T < 360$ K, the electrical conductivities of the lithium triflate-doped POEM-*g*-PDMS, which exhibited solid-like mechanical behavior, were nearly identical to those of the liquid POEM homopolymer. Thermal and electrochemical stability studies showed the electrolyte to be stable over a wide temperature range and voltage window. Solid-state, thin-film batteries comprised of a metallic lithium anode, a ~0.2 μm thick vanadium oxide cathode, and an electrolyte of POEM-*g*-PDMS doped with $LiCF_3SO_3$ proved resistant to capacity fade during extended cycling at room temperature (>200 cycles) at a discharge rate of 2/3 C and could be cycled (charged and discharged) at subambient temperature (0°C).
 [DOI: 10.1149/1.1824032]

Manuscript submitted March 19, 2004; revised manuscript received May 19, 2004. Available electronically November 17, 2004.

The proliferation of portable electronics has brought an increased demand for high-performance rechargeable batteries. Currently, most commercial cells use liquid or liquid-based electrolytes that limit their thermal stability, energy density, and safety.[1] Clearly, performance gains could be made if a dry, solid electrolyte were exploited.

Since the discovery of the ion-conducting properties of doped polyethylene oxide, researchers have searched for a material exhibiting liquid-like ionic conductivity and mechanical properties suitable for separating the electrodes. Work in our laboratory and elsewhere has focused on block copolymer electrolytes (BCEs),[2-12] polymers consisting of two chemically dissimilar chains or ''blocks.'' A net repulsion between the blocks leads them to phase separate locally into nanometer-scale domains, the morphology of which can be controlled by the overall composition of the copolymer.[13] A material thus can be created that has a continuous, amorphous poly(ethylene oxide) (PEO)-rich phase.[3,4] The interfaces between the domains engender solid-like mechanical properties, even if both components are well above their respective glass transition temperatures (T_gs),[14] while locally within each domain the polymer chain mobility remains high.[15] When a lithium salt is added, the polymer becomes a solid electrolyte, behaving mechanically like a rubbery solid but still possessing high ionic conductivity.[4]

In the past, block copolymers of this nature were produced by anionic synthesis, a time-consuming, expensive, laborious process that requires high-purity reagents.[1-12,16] More recently, our group employed atom transfer radical polymerization (ATRP) to create such systems,[3] ameliorating many of these synthesis drawbacks. However, the reaction rates associated with ATRP vary greatly with factors such as temperature and the age of chemicals, and the technique has yet to gain wide-scale acceptance in industry. This paper introduces a novel graft copolymer electrolyte (GCE) created by simple, robust, free radical synthesis (with the aid of a commercially available macromonomer). The material has a backbone composed of the lithium-salt-solvating poly[(oxyethylene)$_9$ methacrylate] (POEM) and long side chains of poly(dimethyl siloxane) (PDMS). The choice of PDMS was motivated by the observation in our BCE studies[4] that the electrical conductivity of these systems scales inversely with the glass transition temperature of the secondary (non-conducting) block.[4,15] With its T_g of -123°C,[17] far lower than that of the alkyl methacrylates used in our previous studies, PDMS was an attractive candidate, expected to impart conductivities higher than previously attained.

Experimental

Poly[(oxyethylene)$_9$ methacrylate]-*g*-poly(dimethyl siloxane) (POEM-*g*-PDMS) (70:30) was synthesized by free radical methods. 6 mL of poly(dimethyl siloxane) monomethacrylate macromonomer (Aldrich, $M_n \approx 10{,}000$ g/mol) and 13 mL of poly(ethylene glycol) methyl ether methacrylate monomer (Aldrich, $M_n = 475$ g/mol) were added to 80 mL of ethyl acetate and stirred (Fig. 1). This formulation corresponds to a weight ratio of 70:30 (POEM:PDMS) or a molar ratio of ~50:1 (POEM:PDMS side chains). Next, 6 mg of the initiator 2,2′-azobisisobutyronitrile (AIBN, Aldrich) were added (825:1 monomer:initiator) and the flask was sealed and purged for 30 min with grade-5 argon. The solution was then heated to 68°C in an oil bath and left under constant stirring. After 24 h, the polymer was precipitated in hexane. The product had a molecular weight of ~480,000 g/mol with respect to a polystyrene calibration curve as determined by gel permeation chromatography (GPC), corresponding to roughly 15 PDMS side chains per molecule.

Thermal analysis of the material was conducted on a TA Instruments, Inc., 2920 differential scanning calorimeter (DSC) and a 951 thermogravimetric analyzer (TGA) equipped with a Nicolet 510P Fourier transform infrared (FTIR) spectrometer to identify gases evolved during thermal decomposition. DSC samples were heated at a rate of 10°C/min in a flowing atmosphere of nitrogen (50 cm^3/min). The samples were encapsulated in aluminum pans tightly fitted with inverted lids to ensure good thermal contact between the sample and the pan. T_g's were determined by the inflection point method. TGA samples were heated in a platinum boat at a rate of 30°C/min with a nitrogen purge (100 cm^3/min). The relatively fast heating rate was used to increase the sensitivity of the FTIR measurements. The TGA module was interfaced directly to the FTIR gas sampling cell, thereby obviating the need for a heated transfer line. This arrangement provided for excellent temporal resolution between the TGA and FTIR signals. FTIR gas-phase spectra were collected at a resolution of 4 cm^{-1} with an MCT/A detector.

Small angle neutron scattering measurements were performed using a pulsed-source time-of-flight instrument, the Low-Q Diffractometer (LQD) at the Manuel Lujan, Jr., Neutron Scattering Center (LANSCE) of the Los Alamos National Laboratory. The LQD pro-

* Electrochemical Society Active Member.
z E-mail: amayes@mit.edu

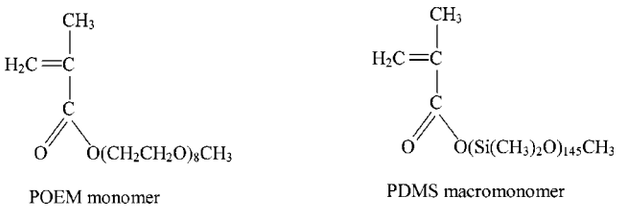

Figure 1. Chemical formulas for POEM and PDMS monomers. The synthesis produces a polymer consisting of a random distribution of these units.

vided data in the q-range of 0.004-0.3 $Å^{-1}$ in a single measurement by using a position-sensitive area detector and neutrons with wavelengths in the range of 1.5-15 Å. All measurements were taken at ambient temperature (25 ± 1°C). The scattering data were corrected for empty quartz-window scattering, detector sensitivity, and sample transmission. The differential scattering cross section $I(q)$ was calculated on an absolute scale in the units of cm^{-1} by using secondary standards whose absolute scattering cross sections were known. As the magnitude of the scattered neutron momentum transfer was measured by time-of-flight techniques, the reduction of data from these instruments included other operations such as projection of the initial data [i.e., $I(\theta,t)$, where θ is the scattering angle and t is the time of flight] onto q space [*i.e.*, $I(q)$]; published methods[18,19] were used for these procedures.

Transmission electron microscopy (TEM) was performed using a JEOL 200CX in bright-field mode operating at 120 keV. TEM specimens were obtained by first securing the polymer onto a metal post using quick-setting epoxy. The sample was then cooled to −85°C, trimmed, and cryomicrotomed into ~30 nm thick sections with the aid of an RMC (Tuscon, AZ) MT-XL ultramicrotome. The thin slices were then mounted on copper grids. The resulting TEM images confirmed the SANS findings and also provided information about the specific morphology of the polymer.

In order to demonstrate the dimensional stability needed for solid-state battery applications, the dynamic properties of the copolymer were probed using a strain-controlled rheometer (ARES, Rheometrics). The rheometer was operated in the parallel-plate oscillatory shear mode with a 1 mm gap. The sample was molded on the 25 mm diam test fixture by pressing a film of the material to the measurement gap width at 90°C. Measurements were performed at 90° and 25°C; the temperature was regulated to within ±1°C using a thermally controlled nitrogen purge. The frequency dependence of the dynamic storage and loss moduli (G' and G'', respectively) were recorded for the frequency range from 200 to 0.1 rad/s at a relatively small strain amplitude of 1.5%. All the data documented were reproducible within an error limit of 5%. Compression studies were also performed with the aid of the rheometer. Circular parallel plates were electrically insulated from one another by fixing a silver-coated mylar film to each 8 mm diam platen. A controlled normal force was applied and the resistance was measured for electrolyte films of varying initial thickness. Higher pressures were also applied using a clamp and a calibrated load cell.

The electrical conductivity was obtained by impedance spectroscopy using a waveform generator/response analyzer (Solartron model 1260 frequency response analyzer, Solartron Analytical, Houston, TX) controlled by a PC running commercially available software (Z60, Scribner Associates, Inc., Southern Pines, NC). The test fixture consisted of two blocking electrodes made of stainless steel and attached to a micrometer which measured the electrode separation, and hence, the thickness of the polymer specimen, which was kept under an atmosphere of flowing argon gas. Polymer films were cast from tetrahydrofuran (THF) and dried under vacuum for 6 h. Increasing the drying time and temperature did not affect the recorded conductivity. Doping with $LiCF_3SO_3$ to obtain a Li:[EO] ratio of 1:20 made the polymer electrolyte conductive.

The electrochemical stability of the GCE was investigated by cyclic voltammetry. The electrolyte was pressed between an oversized counter electrode of lithium and a 1 cm^2 working electrode of platinum to a film thickness of approximately 100 μm. Using a Solartron 1286 electrochemical interface (Solartron Analytical, Houston, TX) controlled by a PC running CorrWare (Scribner Associates, Inc., Southern Pines, NC), the potential was scanned from +2.3 to +5.0 V at a sweep rate of 2 mV s^{-1}.

To study the GCE's performance in a solid-state battery, the electrolyte was incorporated into thin-film test cells fitted with a cathode of vanadium oxide on aluminum foil and an anode of lithium. For the cycling data, vanadium oxide thin films were deposited onto an aluminum foil substrate (area ~1 cm^2, thickness ~20 μm) by ion-assisted, e-beam evaporation of vanadium metal in a controlled oxygen environment. The chamber was kept at 320°C. After deposition, films were annealed at 250°C for 2 h. Oxide film thicknesses were determined to be ~0.2 μm as measured by profilometry. X-ray diffraction (XRD) studies using a rotating anode and Cu Kα radiation (Rigaku RTP500RC) revealed the oxide films to be partially crystalline with broad peaks. Some peaks were identified as V_2O_3, although several others could not be matched to a specific phase, suggesting a mixed phase system. By Auger electron spectroscopy the vanadium concentration of the oxide films was measured as 39 ± 2% on an atomic basis, which puts their stoichiometry between V_2O_3 and V_2O_4; accordingly, we refer to the films simply as VO_x, where $1.5 < x < 2$. Electrolyte films, measuring 2 and 60 μm in thickness for the ambient temperature and varied temperature cycling tests, respectively, were prepared by solution casting from THF directly onto the VO_x film in an argon-filled glove box. The GCE/cathode construct was subsequently dried under vacuum for 4-6 h. Cycle testing was conducted at 25°C with a Maccor series 4000 automated test system. Voltage limits were set at 4.0 and 1.5 V with discharge and charge rates of 2/3 C, where the C/1 rate is defined as a current density of 270 mA/g cathode mass. A second study involved comparing the current capabilities of cells fitted with GCEs of different thicknesses to that of another identical cell containing liquid electrolyte. For this study, vanadium pentoxide cathode films were produced via radio-frequency (rf). sputtering of a 3 in. diam V_2O_5 target in 2% O_2:Ar gas. The substrate current collector consisted of an aluminum foil kept at a constant temperature of approximately 250°C during the course of the deposition. The sputtering gun was kept at a forward power of 300 W. Films were subsequently annealed at 250°C under a flowing oxygen:argon atmosphere and were determined to be V_2O_5 via XRD. Profilometry performed on a dummy silicon wafer showed the thickness to be approximately 375 nm. Again, the Maccor was used at higher current rates while a Solartron 1286 was used at lower currents for improved resolution. Due to systematic error in the Maccor instrument at low current ranges (<100 uA), data obtained from the Maccor was normalized to the Solartron potentiostat through applying a constant current shift of 10 μA/cm^2 across the entire data range. Cells were tested between 2.1 and 3.9 V. Specific current rates were repeated for cells after an entire run to ensure that no capacity fade occurred during the course of the experiment.

Results and Discussion

Figure 2a shows a TGA curve of a POEM-*g*-PDMS sample doped with lithium triflate. (The TGA trace for the pure, undoped polymer was virtually identical). The GCE exhibits excellent thermal stability well above 200°C. The small, low-temperature weight loss is due to the evolution of adsorbed water. FTIR spectra of tetraethylene glycol diethyl ether and hexamethylcyclosiloxane were obtained at approximately 350 and 450°C, indicating the decomposition of the POEM[20] and PDMS[21] components, respectively. The weight losses are in good agreement with the overall composition of the material, noting that the residue of about 3% consisted of black char, a common decomposition product of polymeric materials in an inert atmosphere. The DSC heating curve (Fig. 2b) of the graft co-

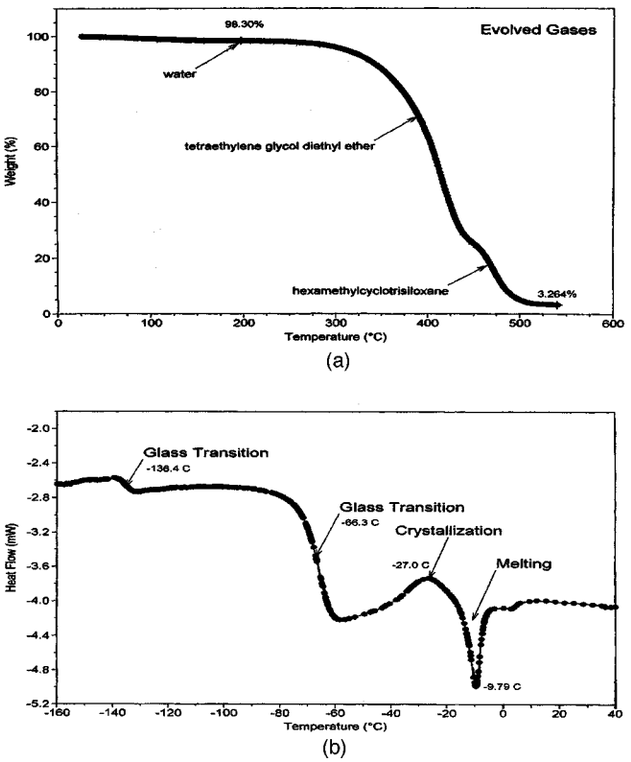

Figure 2. (a) TGA data on POEM-*g*-PDMS system. FTIR spectroscopy identified the evolved gases. (b) A DSC curve of the graft copolymer. Scan rate 10°C/min.

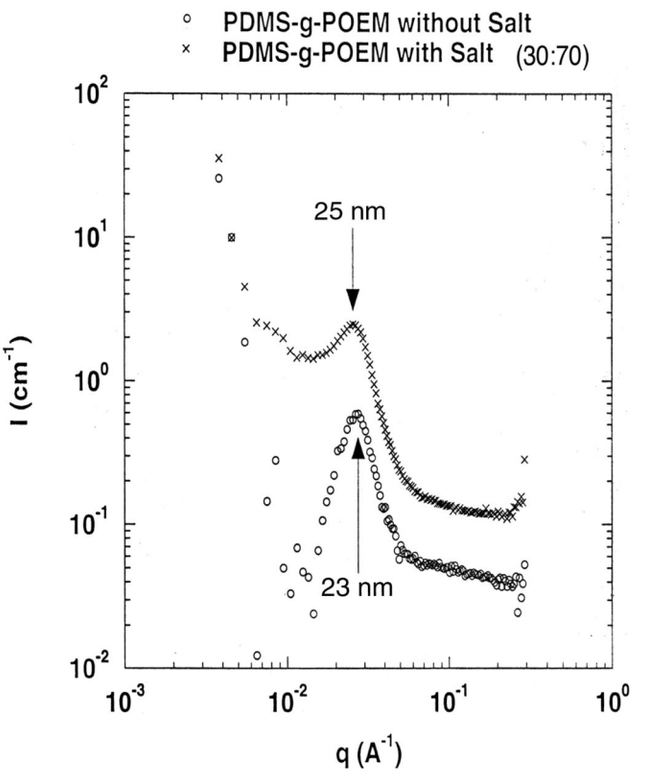

Figure 3. SANS data taken at 20°C on POEM-*g*-PDMS (70:30) and POEM-*g*-PDMS (70:30) doped with $LiCF_3SO_3$ to obtain a Li:[EO] ratio of 1:20. The intense reflection at 0.025 $Å^{-1}$ indicates an ordered morphology having a domain periodicity of ~24 nm.

polymer indicates that the material is microphase-separated, showing two distinct glass transition temperatures at −136 and −66°C that can be attributed to the PDMS and POEM domains, respectively. The exothermic and endothermic peaks at about −27 and −10°C are the result of crystallization and subsequent melting of the PDMS component.

Small-angle neutron scattering data confirm that the material is microphase-separated (Fig. 3). The strong reflection at $q \approx 0.03\ Å^{-1}$ suggests a characteristic domain spacing of approximately 23 nm, a figure consistent with dimensions observed in images obtained via TEM (Fig. 4). The copolymer remains in a microphase-separated state upon the addition of lithium triflate, with an increase in domain periodicity to ~25 nm. The material exhibits a defect-laden, bicontinuous, nanophase morphology (Fig. 4), as seen in other studies on microphase-separating graft copolymers.[13,22,23] The random graft-site distribution perturbs the development of long-range order. Contrast between the PDMS (dark) and POEM (light) domains in Fig. 4 can be attributed to differences in electron density and beam degradation rates.

Because both copolymer blocks are low-T_g polymers, the material's rubbery mechanical properties and excellent dimensional stability originate from the interfaces created by the microphase separation of the POEM backbone and PDMS side chains (Fig. 5). Figure 5 shows the storage (G') and loss (G'') moduli of the graft copolymer as a function of reduced frequency, illustrating the solid-like nature of the material. As is common, the storage moduli, taken at two different temperatures (90 and 25°C), were brought to overlap using the method known as time-temperature superposition, and the loss moduli were shifted correspondingly. Here, the 90°C moduli were referenced with respect to the 25°C data by applying a horizontal shift factor (a_t) of 0.125. The magnitude and frequency dependence of the graft copolymer is nearly identical to that of a poly[(oxyethylene)$_9$ methacrylate]-*b*-poly(lauryl methacrylate) (68:32) system studied previously;[4] the low-frequency behavior suggests that the copolymer exists in a microphase-separated state,[24] and the moduli are sufficiently high for most battery applications. For both materials, the general weak dependence of the moduli on frequency/temperature arises from the fact that the mechanical properties of the system are dictated by the interfaces between the domains. At room temperature each polymer is already well into the melt regime; accordingly, temperature variations have little effect on the overall stiffness of the material.[25]

Compression tests revealed that the material is highly elastic, recovering its initial dimensions upon removal of pressures as high as 40 psi (corresponding to the highest force that could be applied by the apparatus). Undoped graft copolymer films between ~8 and ~190 μm thick were subject to static loading for 1 h. The material

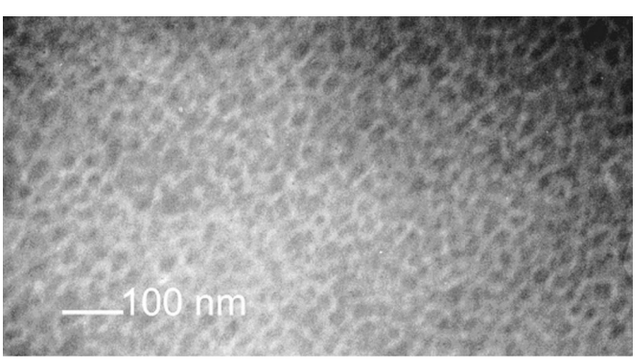

Figure 4. Bright-field TEM micrograph of POEM-*g*-PDMS (70:30). PDMS appears as the darker phase.

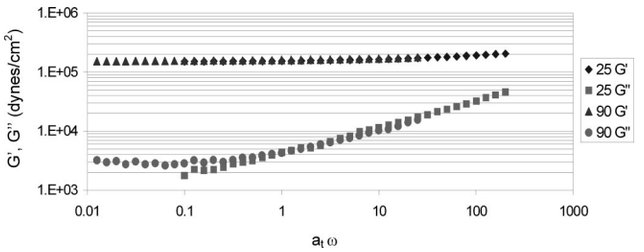

Figure 5. Dynamic frequency sweep testing on POEM-*g*-PDMS with 1.5% strain. Moduli data are shifted to a 25°C reference temperature.

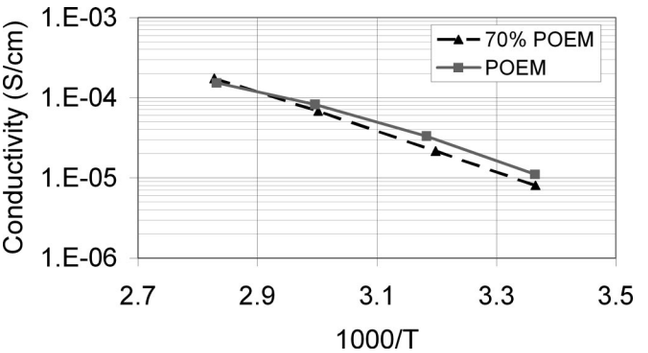

Figure 7. Temperature dependence of electrical conductivity of POEM-*g*-PDMS (70:30) and POEM, each doped with $LiCF_3SO_3$ to a Li:[EO] ratio of 1:20.

was capable of supporting elevated pressures without any detectable creep. Although the electronic resistance of the sample did decrease due to the thickness change that accompanied the loading, the films always possessed more than adequately high values to prevent shorting. Subsequent tests were done with 0.3 $in.^2$ samples (200 μm thick, stainless steel electrode plates) using a clamp and a load cell to measure the applied force. At a pressure of ~60 psi, the copolymer exhibited limited plastic flow. However, after an initial irreversible deformation the material was able to maintain the pressure for 15 min, which was the duration of the experiment. At 120 psi, when the film dimensions stabilized, the resistance still exceeded 100 kΩ. Visible inspection of the film after the test revealed substantial nonuniform thinning (average thickness ~10 μm). These results suggest that (neglecting any margin of safety) the GCE can be processed or used at pressures approaching 60 psi. Beyond that threshold, the cell still should not short immediately, but its dimensions and integrity would begin to be compromised.

Cyclic voltammetry performed at room temperature demonstrated the electrolytic stability of the salt-doped graft copolymer (Fig. 6). Small currents were measured at extreme potentials, *e.g.*, ~2.5 $\mu A/cm^2$ at 5.0 V. Apart from a slight rise in current at ~4.0 V believed to be associated with the breakdown of the lithium salt, there was no evidence of significant electrochemical activity in the polymer at potentials as high as 5 V.

Figure 7 shows that over the temperature range $290 < T < 360$ K, the electrical conductivities of the GCE and the salt-doped molten POEM homopolymer, both exhibiting the expected Vogel-Tammann-Fulcher behavior, are almost identical. This illustrates the benefit of including a low T_g nonconducting domain: comparable conductivity combined with dimensional stability. Replacing lithium triflate with a more conductive imide salt, increasing the fraction of POEM, or incorporating oligomeric PEO would raise the GCE conductivity still higher. Furthermore, because the GCE film can be made very thin, the overall resistance can be kept acceptably low for battery use even at the reported values of electrical conductivity.

To confirm the viability of the GCE, a solid-state cell was constructed with a VO_x cathode, lithium anode, and 2 μm electrolyte film. Cycle testing at a current rate of 2/3 C (200 mA/g) between 1.5 and 4.0 V revealed a first discharge capacity of 50 mAh/g. Further cycling caused the discharge capacity to increase substantially. This result may be attributable to improved contact between components of the cell. Alternatively, we speculate that the enhanced capacity on cycling may be due to orientation of the GCE domains under the applied potential, causing a reduction of the interfacial impedance between the electrolyte and electrode. Block copolymer domain orientation under applied electric fields has been observed previously, for example, by Thurn-Albrecht *et al.* in their work with polystyrene-*b*-poly(methyl methacrylate).[26] Figure 8 shows the evolution of the discharge capacities for a cell cycled at 2/3 C for 200 cycles. While an initial capacity of ~50 mAh/g was measured, this rose monotonically and reached a steady-state value of ~180 mAh/g after 15 cycles. These results suggest that a further attribute of this electrolyte may be the ability to self-optimize its morphology in service.

The effect of bulk electrolyte resistance on cell performance was probed by studying several cells constructed with different polymer thicknesses ranging from 13 to 127 μm. These batteries, fitted with V_2O_5 sputtered cathodes, were cycled at assorted discharge rates and their performance was compared to that of a cell made with liquid electrolyte. Although capacity was seen to decrease at higher current rates (as expected), there was no appreciable difference in performance between any of the cells (Fig. 9); the rate-limiting step in these microbattery geometries does not appear to be related to the lithium-ion transport through the electrolyte.

In an effort to investigate the relationship between battery performance and temperature, cells fitted with a GCE of thickness ~60 μm and liquid electrolyte (EC:DEC) were cycled at subambient temperatures (10 and 0°C) and at elevated temperature

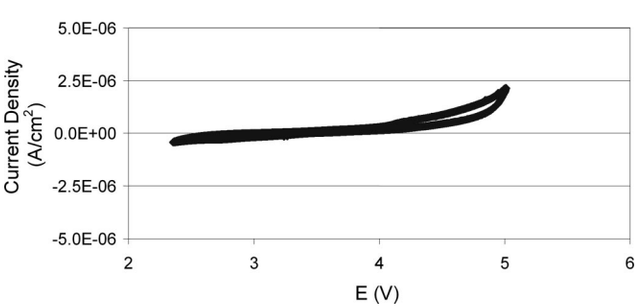

Figure 6. Cyclic voltammetry of doped POEM-*g*-PDMS using a platinum working electrode and lithium counter electrode.

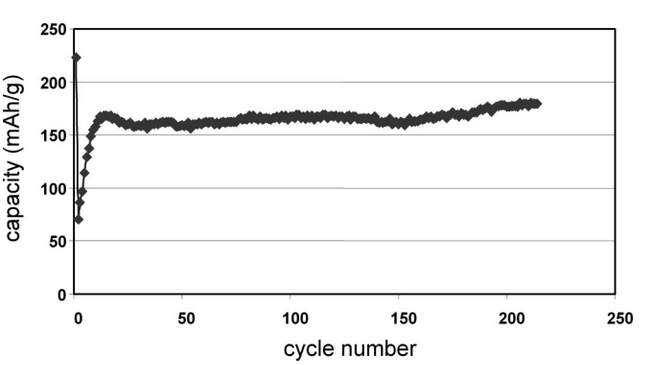

Figure 8. Room-temperature cycling of a solid-state battery of Li/POEM-*g*-PDMS (70:30)/VO_x. GCE film thickness ~2 μm.

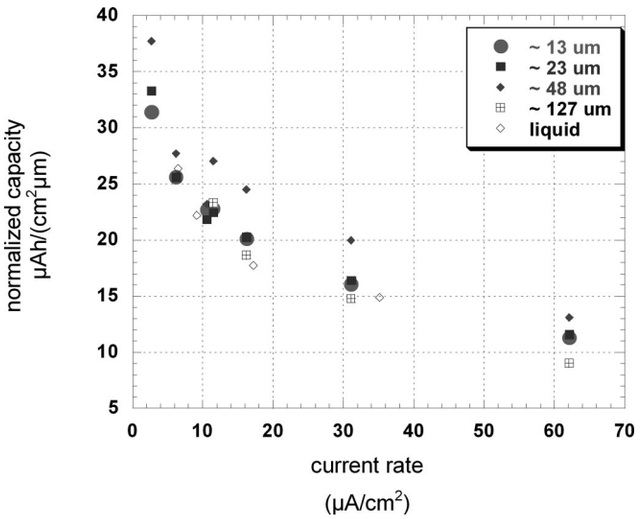

Figure 9. Normalized capacity as a function of current rate and electrolyte thickness for POEM-*g*-PDMS. Liquid electrolyte data are included for comparison.

(~52°C), always at a rate of 2/3 C (Fig. 10). The capacity data in Fig. 10 have been normalized to account for variations between cathodes. The capacity of the cells decreased upon lowering the temperature, presumably due to rate limitations associated with processes occurring at (or inside) the electrodes, because as seen previously, even huge changes in the bulk electrolyte resistance did not impact the batteries' performance. The GCE cell's behavior was monitored as it warmed from 0°C (Fig. 10b). The consistency in the cell's performance at room temperature demonstrated that the capacity was recoverable. Upon heating to 52°C, the liquid-electrolyte-containing cell experienced rapid capacity fade before it failed abruptly. Inspection of the disassembled battery revealed that the cathode had dissolved into the electrolyte leaving the current collector nearly bare. The graft-copolymer-electrolyte battery fared better at elevated temperature, exhibiting much less capacity fade. These findings are consistent with those published by Lee *et al.*:[27] amorphous vanadium oxide films dissolve in liquid electrolyte unless a solid-electrolyte layer is used as a protective coating.

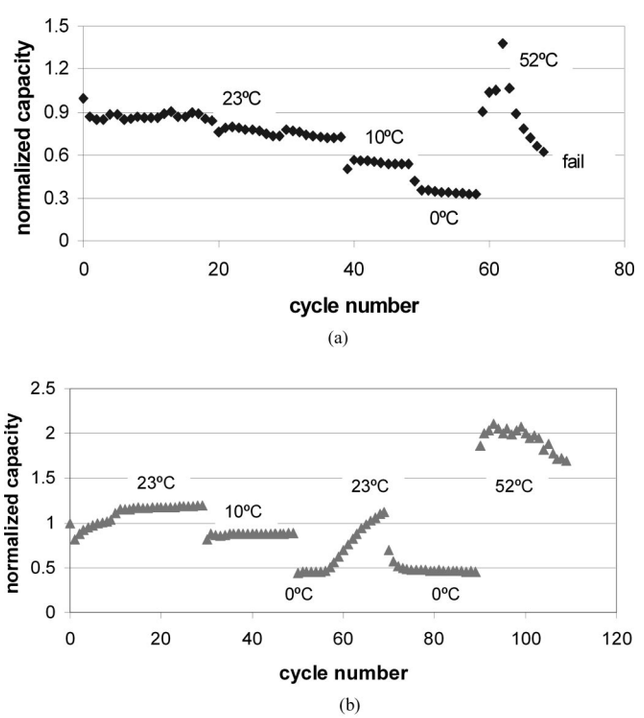

Figure 10. Cycle testing of two Li/electrolyte/VO_x batteries, (a) one with a liquid (EC:DEC) electrolyte and (b) one with a graft copolymer (70:30 POEM-*g*-PDMS), doped with $LiCF_3SO_3$ to a Li:[EO] ratio of 1:20.

The graft copolymer electrolyte investigated in this work possesses the best combination of electrical and mechanical properties of the salt-doped materials examined to date in our laboratory. In parallel, the GCE can be produced by simple and scalable synthesis.

Acknowledgments

This work was sponsored by the Office of Naval Research under contracts N00014-99-1-0561, N00014-99-1-0565, N00014-00-1-0356, and N00014-02-1-0226; the MRSEC Program of the National Science Foundation under awards DMR-988089431 and DMR-0213282; and Intronics Corporation. The authors acknowledge Peter O'Brien and Roshan Aggarwal of MIT Lincoln Laboratory for providing vapor-deposited vanadium oxide films. This work has benefited from the use of Los Alamos Neutron Science Center at the Los Alamos National Laboratory. This facility is funded by the U.S. Department of Energy under contract W-7405-ENG-36. This report presents the views of the authors only, not those of their sponsors.

Massachusetts Institute of Technology assisted in meeting the publication costs of this article.

References

1. P. V. Wright, *MRS Bull.*, **27**, 597 (2002).
2. J. Saunier, F. Alloin, and J. Y. Sanchez, *Electrochim. Acta*, **45**, 1255 (2000).
3. P. E. Trapa, B. Huang, Y.-Y. Won, D. R. Sadoway, and A. M. Mayes, *Electrochem. Solid-State Lett.*, **5**, A85 (2002).
4. P. P. Soo, B. Huang, Y.-I. Jang, Y.-M. Chiang, D. R. Sadoway, and A. M. Mayes, *J. Electrochem. Soc.*, **146**, 32 (1999).
5. H. R. Allcock, R. Prange, and T. J. Hartle, *Macromolecules*, **34**, 5463 (2001).
6. F. M. Gray, J. R. MacCallum, C. A. Vincent, and J. R. M. Giles, *Macromolecules*, **21**, 392 (1988).
7. J. R. M. Giles, F. M. Gray, J. R. MacCallum, and C. A. Vincent, *Polymer*, **28**, 1977 (1987).
8. I. M. Khan, D. Fish, Y. Delaviz, and J. Smid, Makiromol. Chem., **190**, 1069 (1989).
9. J. Li and I. M. Khan, *Makromol. Chem.*, **192**, 3043 (1991).
10. S. Kohjiya and Y. Ikeda, *Materials Science Research International*, **4**, 73 (1998).
11. M. Watanabe, S. Oohashi, K. Sanui, N. Ogata, T. Kobayashi, and Z. Ohtaki, *Macromolecules*, **18**, 1945 (1985).
12. A.-V. G. Ruzette, P. P. Soo, D. R. Sadoway, and A. M. Mayes, *J. Electrochem. Soc.*, **148**, A537 (2001).
13. M. Xenidou, F. L. Beyer, N. Hadjichristidis, S. P. Gido, and N. B. Tan, *Macromolecules*, **31**, 7659 (1998).
14. F. S. Bates, H. E. Bair, and M. A. Hartney, *Macromolecules*, **17**, 1987 (1984).
15. D. J. Harris, T. J. Bonagamba, K. Schmidt Rohr, P. P. Soo, D. R. Sadoway, and A. M. Mayes, *Macromolecules*, **35**, 3772 (2002).
16. H. L. Hsieh and R. P. Quirk, *Anionic Polymerization: Principles and Practical Applications*, Marcel Dekker, Inc., New York (1996).
17. S. J. Clarson, K. Dodgson, and J. A. Semlyen, *Polymer*, **26**, 930 (1985).
18. P. A. Seeger, *J. Appl. Crystallogr.*, **21**, 613 (1988).
19. R. P. Hjelm, Jr., *J. Appl. Crystallogr.*, **20**, 273 (1987).
20. T. Shodai, B. B. Owens, H. Ohtsuka, and J.-I. Yamaki, *J. Electrochem. Soc.*, **141**, 2978 (1994).
21. S. J. Clarson and J. A. Semlyen, *Polymer*, **27**, 91 (1986).
22. J. F. Hester, P. Banerjee, Y. Y. Won, A. Akthakul, M. H. Acar, and A. M. Mayes, *Macromolecules*, **35**, 7652 (2002).
23. T. Miyata, S. Obata, and T. Uragami, *Macromolecules*, **32**, 8465 (1999).
24. J. H. Rosedale and F. S. Bates, *Macromolecules*, **23**, 2329 (1990).
25. J. D. Ferry, *Viscoelastic Properties of Polymers*, 3rd ed., Wiley, New York (1980).
26. T. Thurn-Albrecht, J. DeRouchey, T. P. Russell, and H. M. Jaeger, *Macromolecules*, **33**, 3250 (2000).
27. S.-H. Lee, H. M. Cheong, P. Liu, and C. E. Tracy, *Electrochem. Solid-State Lett.*, **6**, A102 (2003).